Journal of Analytical and Applied Pyrolysis 140 (2019) 102–111

Contents lists available at ScienceDirect

Journal of Analytical and Applied Pyrolysis

journal homepage: www.elsevier.com/locate/jaap

Exploring the composition of macromolecular organic matter in Arctic Ocean sediments under a changing sea ice gradient

Mark A. Stevenson*, Geoffrey D. Abbott

School of Natural and Environmental Sciences, Drummond Building, Newcastle University, Newcastle upon Tyne, NE1 7RU, UK

ARTICLE INFO

Keywords:
Arctic ocean
Barents Sea
Carbon cycling
Marine sediment
Macromolecular organic matter
Sea ice retreat

ABSTRACT

Arctic sea ice has been affected by climate change, leading to reductions in summer sea ice extent over the past few decades, impacting nutrient dynamics, ocean temperature fluxes and the biological communities present in the ocean. Marine organic matter is a complex mixture of differentially degraded terrestrial and marine organisms from a range of sources and time periods. In this study pyrolysis-gas chromatography-mass spectrometry (Py-GC–MS) has been used to quantify the solvent-insoluble component of marine organic matter in surface sediments to gain a more holistic understanding of the macromolecular composition at five stations along a south to north transect in the Arctic Barents Sea, east of Svalbard (depths 288–334 m.b.s.l). Two methods were compared to identify the effectiveness of rapid screening, in contrast to grouping similar pyrolysis products. There were changes in macromolecular composition of marine surface sediments across the S-N transect using both methods, highlighting the varying benthic and pelagic communities north of the Polar Front and across the variable sea ice margin, corresponding to differing biological communities (e.g. fish, phytoplankton, ice algae, zooplankton). All five stations across the changing sea ice transect were interpreted as having primarily marine surface sediment macromolecular signatures, given their locations far from major terrestrial inputs and the more subtle changes when compared with previous investigations on the East Siberian Artic shelf. Fluctuations in macromolecular compositions across the transect included increasing N-containing compounds (including pyridines) and *n*-alkene/*n*-alkane doublet pyrolysis products from sediments collected in stations with the greatest average ice cover. If the future position of the Polar Front moves northwards then deposition of labile organic matter which appears to be efficiently processed will move further north, meaning greater deposition of organic carbon under areas of open ocean. Future research needs to understand how this OC will be buried and if it is regionally significant, given anticipated weakening stratification and a more Atlantic influenced northern Barents Sea.

1. Introduction

Warming linked to recent climate change has been greatest in the Arctic leading to pronounced reductions in sea ice extent and thickness [1,2]. Changes in the timing, extent and thickness of sea ice have complex effects on ocean stratification, currents and temperature leading to variations in algal abundance and the composition of producers and consumers present at all depths [3,4]. For example, presence of sea ice can help maintain stratification of the water column as freshwater input helps maintain the less saline Arctic layer associated with seasonal melt. In the northern Barents Sea weakening stratification is presently resulting in a transition from a stratified Arctic ocean, to a more Atlantic influenced system [5,6]. While the trend towards decreasing sea ice is expected overall to increase Arctic primary productivity [7], the changing position of the ice edge is a key location of production due to the supply of nutrients and upwelling which has the potential to complicate trends.

Ocean sediments contain organic carbon that has been cycled through the marine food web, or delivered through ocean currents from terrestrial sources. In order to accurately understand how sea ice retreat might influence the quality of carbon burial at the ocean floor, it is important to validate the potential available quantification approaches. While the majority of studies use organic geochemical techniques to characterise the solvent-soluble component of marine organic matter (OM), these approaches ignore the substantial and often greater quantity of residual OM present in the solvent-insoluble fraction. The solvent-insoluble fraction is important both because it can contain particles transported by ocean currents that are hydrodynamically sorted [8]

* Corresponding author.
E-mail address: mark.stevenson@ncl.ac.uk (M.A. Stevenson).

https://doi.org/10.1016/j.jaap.2019.02.006
Received 31 August 2018; Received in revised form 21 January 2019; Accepted 13 February 2019
Available online 14 February 2019

and since it contains a broader suite of representative compounds, compared with studies focused solely on the solvent-soluble fraction. Pyrolysis is ideally suited to the characterisation of macromolecular OM, whereby oligomers or polymers are thermally fragmented into volatile components amenable by gas chromatography-mass spectrometry, to provide evidence of broad changes in multiple pyrolysis product compound classes.

Previous studies which have applied macromolecular pyrolysis techniques to ocean sediments have focused either on broad coastal to oceanic gradients [9–11] or where specific differences exist between overlying bottom water mass composition, such as the presence of an extended oxygen minimum zone [12]. In this study we focus on a N-S transect (30 °E) spanning five stations from 74 °N to 81 °N across the Barents Sea continental shelf, where variations in macromolecular composition are expected to be more subtle, necessitating a comparison of quantification approaches. This transect spans a region where warmer Atlantic water from the south-west meets cooler Arctic currents flowing from the north and is known as the Polar Front. By controlling for depth (range 359–283 m.b.s.l), selecting ocean floor depressions of sediment focusing and assigning stations across a transect encompassing a range of potential sea ice maxima and minima, our analyses focus on sites where qualitatively the major driver of ocean carbon cycling is the extent and duration of sea ice cover. Generally, sea ice cover is greater further north, but due to variability the extent, thickness and drift of sea ice varies between years [13], with a present trend towards warming [5], so robust investigations which characterise sediment macromolecular composition using pyrolysis products help describe changes in carbon burial quality as a result of changes to the trophic character of the water column.

The uppermost layer of marine surface sediment (0.5 cm) focused on in this study represents the most recent deposits, and has been subject to less transformation and diagenesis than deposits beneath. Despite this, the uppermost layer which forms the sediment-water interface in these locations with relatively low deposition rates is still a time-integrated combination of multi-year deposition. The quantification approaches compared in this study both use relative abundances of pyrolysis products detected using specific ions, to facilitate proportional comparisons between samples as flash pyrolysis typically yields a large number of complex, sometimes convoluted ion chromatograms.

Here we compare a method which groups a large number of pyrolysis products into class groups for interpretation [12], in comparison to an approach which uses just one or two key indicator compounds per class for rapid screening [9]. Overall, we aimed to test the applicability of these two methods for understanding ocean sediment macromolecular composition, along a changing sea ice transect, where we expected relatively subtle differences between stations. From these analyses we sought to make provisional interpretations on benthic productivity and organic matter source between ocean floor sampling stations. We expected that both approaches would provide valuable insight for disentangling terrestrial from marine sourced organic matter, but that including more compounds would make differences between class groups more pronounced.

2. Materials and methods

2.1. Study sites and sampling

Samples were obtained on board RRS James Clark Ross cruise JR16006 in July 2017 from the Barents Sea. Detail on the oceanographic cruise and accompanying data is available in the JR16006 cruise report [14]. All samples were sub-sectioned from the uppermost 0.5 cm of a multicorer deployment at depths on the continental shelf ranging from 283 to 359 m.b.s.l. The five stations (named B13–B17) were selected on a 30 °E south to north transect (Fig. 1) to encompass a changing sea ice transect. Cores were sliced onboard the vessel into previously ashed foil and immediately frozen (−80 °C), transported and stored (−20 °C) prior to sub-sectioning and freeze drying. Samples were homogenised (agate pestle and mortar) and stored at (−20 °C) prior to extraction.

2.2. Total organic carbon (TOC) analysis

Freeze dried sediments were acidified using 4 mol. HCL to remove carbonates for 4 h, dried overnight at 60 °C and analysed on a CS230 Carbon/Sulfur Determinator using porous crucibles (Leco Corporation, Michigan, USA). Two surface samples were analysed in triplicate and provided standard deviations < 0.1% TOC. Reported values are the mean of two or three replicates.

2.3. Isolation of marine organic matter (MOM)

Isolation of solvent-insoluble MOM was performed with ~1 g of freeze dried sediment using a Soxtec™ automated extraction system (FOSS North America, Eden Prairie MN) in previously extracted thimbles. Solvent extraction was with dichloromethane:methanol (93:7 (v/v)) using a program of 2 h 10 min at 125 °C, followed by 10 min cooling, repeated twice. Solvent-insoluble MOM was air dried overnight and stored at room temperature in foil capped glass vials prior to analysis.

2.4. Pyrolysis-gas chromatography–mass spectrometry

Online pyrolysis-gas chromatography-mass spectrometry (Py-GC–MS) was conducted in triplicate using the analytical setup described in Abbott et al. [19] with modified run conditions. Samples were weighed (c.a. 10–15 mg) into clean quartz pyrolysis tubes and plugged with solvent extracted silica wool. To assess machine stability a known amount of internal standard (5α-androstane) was added prior to pyrolysis. Py-GC–MS was performed using a pulsed-mode open pyrolysis system in a CDS 1000 pyroprobe unit (CDS Analytical, USA) fitted with a platinum coil and a CDS 1500 valved interface (320 °C) connected to a HP 6890GC split injector (320 °C) linked to a HP 5973 MSD (electron voltage 70 eV, emission current 35 uA, source temperature 230 °C, quadrupole temperature 150 °C, multiplier voltage 2200 V, interface temperature 320 °C). Curie-point flash pyrolysis was conducted at 610 °C for 10 s (20 °C/ms temperature ramp) with products passed onto a Phenomenex ZB-5MS (Torrance, CA, USA) 60 m fused silica capillary column (0.25 mm i.d) coated with 0.25 µm 5% phenyl methyl silicone using helium as the carrier gas (1 mL min^{-1}). The GC program was held at 40 °C for 5 min. and then temperature programmed from 40 °C–48 °C at 2 °C/min, then 48 °C–250 °C at 4 °C/min, then 250 °C–320 °C at 20 °C/min and held at a final temperature for 10 min. The HP 5973 MSD was operated in full scan mode (*m/z* 50–650) and Chemstation was used for data acquisition. All Py-GC–MS samples were analysed in triplicate to ensure analytical reproducibility and enable the presentation of standard deviations.

2.5. Quantification approaches and data display

2.5.1. Method A

Following Nierop et al. [12] chromatograms from each station were explored in triplicate for 78 pyrolysis product compounds with 59 present and quantified in Barents Sea sediments. Identification of compounds was aided by the NIST 98 mass spectral library or by combining spectra with retention time after reference to literature data [9–12]. Peak integration of two main fragment ions for each compound was used for quantification (Table 1) and relative abundances were summed into pyrolysis product compound class groups. In total, 6 of the 8 groups reported in Nierop et al. [12] were present (alkylphenols, other N containing compounds, alkylbenzenes, polysaccharides, alkylpyrroles and *n*-alkenes & *n*-alkanes (C_{10}-C_{23})) and results were reported as relative abundances.

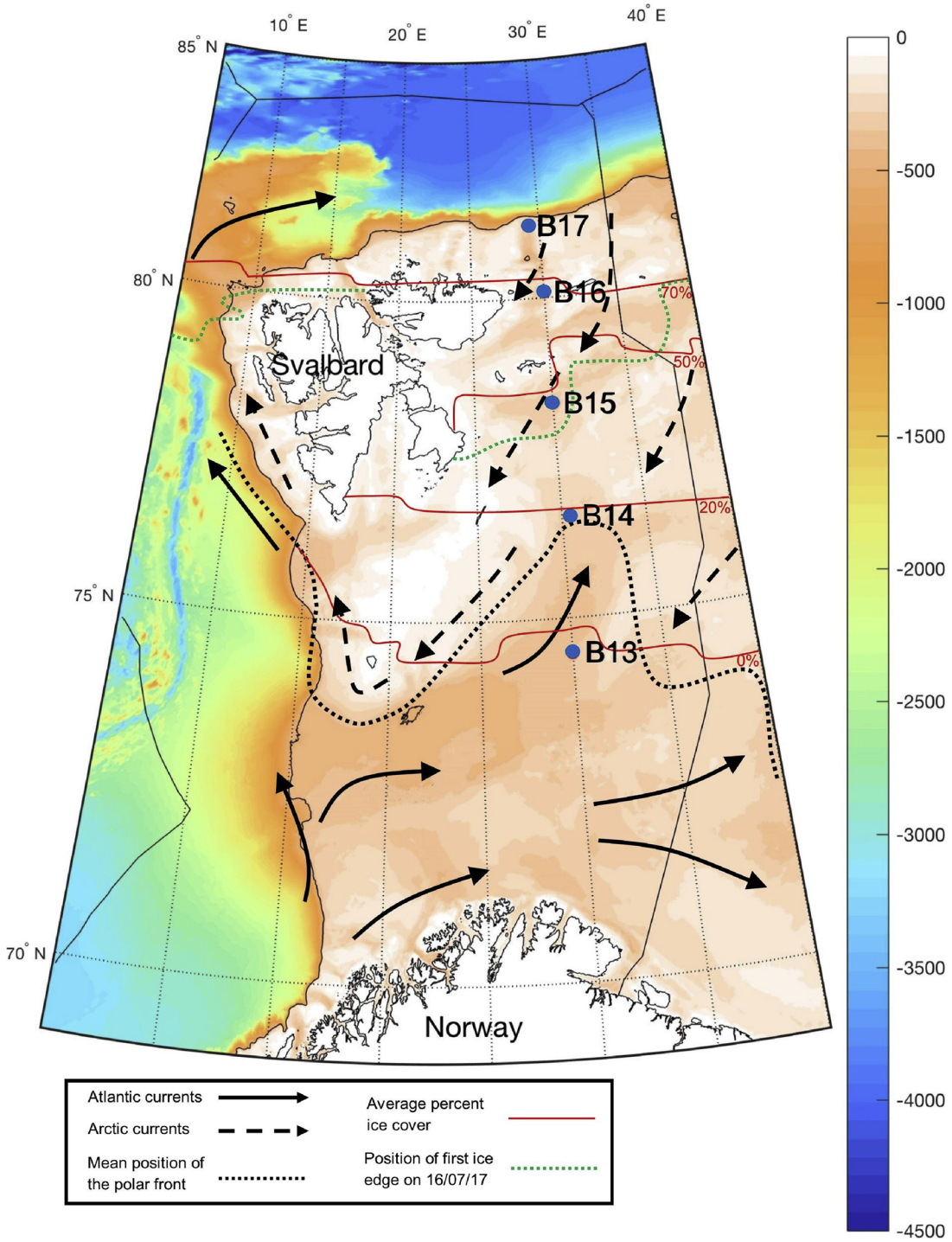

Fig. 1. Location of Barents Sea shelf stations B13–B17 sampled in July 2017 within the Norwegian sector. Bathymetric depth chart indicating meters below sea level (m.b.s.l). Depths of sampling were 359 m at B13 (74° 29.998 N; 30° 00.009 E), 293 m at B14 (76° 30.055 N; 30°30.241E), 317 m at B15 (78° 15.100 N; 30° 00.540 E), 283 m at B16 (80° 07.154 N; 30° 04.069 E) and 340 m at B17 (81° 16.765 N; 30° 19.496 E). Base map adapted with permission from Hopkins et al. [14], using bathymetry from Jakobsson et al. [15]. Position of Atlantic/Arctic currents and the mean position of the Polar Front from Fossheim et al. [16]. Average percent ice cover from Maiti et al. [17] and Keup-Thiel et al. [18]. Position of first ice margin on 16/07/17 sourced from OSI SAF ice edge data (EUMETSAT).

2.5.2. Method B

Following Sparkes et al. [9] single ion filtering was used to measure the specific ion peak area of 9 pyrolysis product compounds (in triplicate) to represent 6 compound classes, which can be linked to marine or terrestrial sources of macromolecular material. This approach uses relative abundances but is uncorrected and so although the relative area of the major ions integrated does not correspond to an actual abundance, it can help to provide differentiation between samples [10,11]. Similar to method A, compound identification was aided by the NIST mass spectral library or by combining spectra with retention time after reference to literature data. Compound groups integrated (Table 1) were the same as in Sparkes et al. [9] and included phenol, two

Table 1
Specific grouped pyrolysis product compounds included in methods A and B and the specific ions used for quantification (*m/z*).

Method A Group	Alkylphenols	*m/z*	Other N containing compounds	*m/z*	Alkylbenzenes	*m/z*	Polysaccharides	*m/z*	Alkylpyrroles	*m/z*	*n*-Alkenes & *n*-Alkanes	*m/z*
Specific compounds included	Phenol	66,94	Indole	90,117	Toluene	91,92	2-Furaldehyde	95,96	Pyrrole	52, 67	C_{10}–C_{23} *n*-alke-1-enes	55,57
	2-Methylphenol	107,108	3-Methyindole	130,131	1,2-Dimethylbenzene	91,106	5-Methyl-2-furaldehyde	109,110	2-Methylpyrrole	80,81	C_{10}–C_{23} *n*-alkanes	57,71
	3- and 4-Methylphenol	107,108	Pyridine	52,79	1,3-Dimethylbenzene	91,106			3-Methylpyrrole	80, 81		
	2-Ethylphenol	107,122	2-Methylpyridine	66,93	Ethylbenzene	91,106			2,5-Dimethylpyrrole	94,95		
	3-Ethylphenol	107,122	3-Methylpyridine	96,66	1,2,3-Tribenzene	105,120			2-Ethylpyrrole	80,95		
					1,2,4-Tribenzene	105,120			3-Ethylpyrrole	80,95		
					1,2,3,4-Tetramethylbenzene	119,134			Trimethylpyrroles	108,109		
					1,2,3,5-Tetramethylbenzene	119,134			4-Ethyl-2-methylpyrrole	94,109		
Method B Group	Phenol	*m/z*	2 Pyridines	*m/z*	Dimethylbenzene	*m/z*	Methylcyclopentenone	*m/z*	2 Furfurals	*m/z*	2 Aromatics	*m/z*
Specific compounds included	Phenol	94	Pyridine	79	Dimethylbenzene	106	Methylcyclopentenone	96	Furfural	96	Indene	116
			Methyl pyridine	93					Methyl furfural	110	Naphthalene	128

pyridines, dimethylbenzene, methylcyclopentenone, two furfurals and two aromatics.

2.5.3. Data display

For *n*-alkene/*n*-alkane distributions compound range *n*-C_{10} to *n*-C_{23} were included in method A to reflect algal contributions [12], but for completeness higher molecular weight *n*-alkanes (*n*-C_{24} to *n*-C_{26}) have also been displayed in relative abundance graphs.

To facilitate comparison in changes across the changing sea ice transect similar groups of pyrolysis product compounds were plotted together from methods A and B including alkylphenols/phenol, other N compounds/2 pyridines, alkylbenzenes/dimethylbenzene and polysaccharides/methylcyclopentenone. Alkylpyrroles (method A), *n*-alkene/*n*-alkane doublets (method A), 2 furfurals (method B) and 2 aromatics (method B) were plotted separately as these compound groups differed substantially between approaches.

3. Results

3.1. Compounds detected

Specific pyrolysis product compounds detected from Py-GC–MS are listed in Table 1, with their position in the chromatogram indicated on Fig. 2. Relative abundances of each individual replicate pyrolysis product and groups of pyrolysis products together with calculated mean, standard deviation (SD) and percentage coefficient of variation (CV) (also termed percentage relative standard deviation (RSD)) are provided in SI Table S1 (Method A) & S2 (Method B). Histograms display the proportional contribution from each group of compounds from methods A and B (Fig. 3). For method A 59 compounds in total were detected in Arctic Ocean (Barents Sea) sediments of the 78 reported in Nierop et al. [12] from the Arabian Sea. In contrast to Nierop et al. [12] prist-1-ene and phytadienes were not detected in the solvent insoluble fraction. Although prist-2-ene was present, it is not included as our aim was to replicate the existing method as closely as possible. For method B all 9 compounds were detected in Arctic Ocean (Barents Sea) sediments, the same as reported in Sparkes et al. [9] for sediments across the East Siberian Arctic Shelf. Aromatic moieties dominated the pyrolysis program (alkylbenzenes, furans, pyranes, alkylpyrroles, alkylpyridines, alkylindoles, alkylphenols) and a homologous series of *n*-alkene/*n*-alkane doublets (Table 1; Figs. 2 and 3).

Among all samples the alkylbenzenes toluene (12.1–18.7%; 12% CV) dominated the chromatograms, followed by 1,2-dimethylbenzene (2.5–3.8%; 13% CV), ethylbenzene (1.4–2.6%; 14% CV), 1,3-dimethylbenzene (1.4–2.3%; 12% CV) and 1,2,3/1,2,4-tribenzenes (0.8–1.3%; 20% CV & 0.6–1.3%; 19% CV respectively). 1,2,3,4 and 1,2,3,5-tetramethylbenzenes (0.4–1.0%; 31% CV & BDL-0.3%; 22% CV) were also present but at lower abundance. Among N-containing compounds pyridine (11.6–23.2%; 27% CV) and 3-methylpyridine (4.5–8.8%; 18% CV) were present in greatest abundance, with indole (0.4–1.8%; 39% CV) and 3-methylindole (0.04-0.27%; 42% CV) also detected but at lower abundance. The heterocyclic pyrolysis products 2-furaldehyde (6.3–20.3%; 37% CV) and 5-methyl-2-furaldehyde (2.1–5.9%; 22% CV) were also present and classified as likely products of polysaccharides. In the alkylphenols group 3- and 4-methylphenols (1.3–5.9%; 34% CV) which co-eluted in our program together with phenol (4.0–7.6%; 13% CV) and 2-methylphenol (0.4–1.8%; 27% CV) were most abundant. The alkylphenols were supplemented at the southernmost stations by lower abundances of 2-ethylphenol (B13 & B14) (0.7–1.5%; 36%) and 3-ethylphenol (B13) (0.6-0.7%; 49% CV). Also present at all stations were the alkylpyrroles 2-methylpyrrole (1.5–4.5%; 37% CV), 3-methylpyrrole (2.0–4.4%; 26% CV) and pyrrole (6.0–9.1%; 15% CV), with at the southernmost stations B13 and B14 2,5-dimethylpyrrole (0.6–4.7%; 118% CV), 2-ethylpyrrole (0.5–0.9%; 25% CV) and 3-ethylpyrrole (0.3–0.4%; 8% CV), together with trimethylpyrroles (0.4–0.3%; 17% CV) at B14.

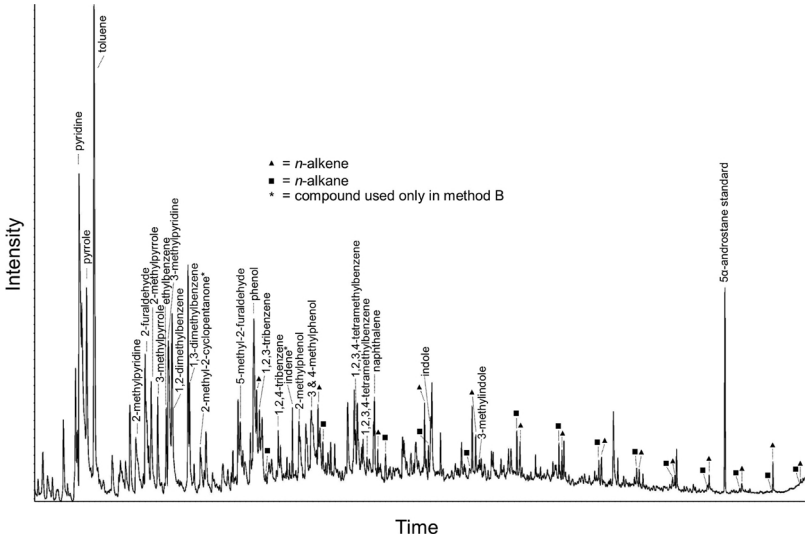

Fig. 2. Labelled chromatogram showing pyrolysis product compounds identified as listed in Table 1.

3.2. Proportional comparisons

3.2.1. Method A

'Other N compounds' comprised the most abundant mean contributions overall (33.1–22.0%), followed by alkylbenzenes (28.7–22.3%) (Fig. 3a). Proportionally, other N compounds were a minimum mean of 22.0% (± 1.0% SD; 5% CV) at B13 and a maximum mean of 33.1% (± 1.7% SD; 5% CV) at B16. The *n*-alkene/*n*-alkane doublets (C_{10} to C_{23}) ranged from a mean of 4.7% (0.2% SD; 5% CV) at B17 to 5.8% (± 0.6% SD; 11% CV) at B16, while alkylpyrroles ranged from a mean of 17.7% (± 2.9% SD; 16% CV) at B13 to 10.6% (± 0.8% SD; 8% CV) at B15.

3.2.2. Method B

For method B the two summed pyridines comprised the most abundant mean contributions at all stations (52.4% (± 3.5% SD; 7% CV) – 38.5% (± 1.2% SD; 3% CV)), followed by 2 furfurals (21.1% (± 6.2% SD; 29% CV) – 35.4% (± 4.7% SD; 9% CV). Dimethylbenzene, the 2 aromatics and methylcyclopentenone had relatively minor contributions at all stations (range 6.3–1.6%), while phenol had a moderate contribution between 11.8% (± 2.4% SD; 20% CV) and 20.6% (± 1.0% SD; 4% CV).

3.3. Compositional changes across the S-N transect

3.3.1. TOC

TOC values were higher in the southernmost stations (B13 = 2.2%; B14 = 2.5%), compared with stations to the north of and including B15 (range 1.6–1.7%) (Fig. 4).

3.3.2. Method A

Alkylphenol pyrolysis product contributions northwards, quantified using the two main specific ion peaks (Table 1) were lowest at station B15 (8.5% (± 2.5% SD; 29% CV), compared with higher ratios in the two most southerly stations (B13 = 14.5% (± 0.5% SD; 3% CV); B14 = 14.5% (± 0.5% SD; 3% CV)) and northernmost stations (B16 = 10.3% (± 1.1% SD; 11% CV); B17 = 10.4% (± 0.1% SD; 1% CV)) (Fig. 4a). Similarly lowest alkylbenzene contributions were at station B15 (22.3% (± 3.1% SD; 14% CV), compared with greater contributions in the southerly stations (B13 = 28.7% (± 0.8% SD; 3% CV); B14 = 28.3% (± 0.8% SD; 3% CV)) and northerly stations (B16 = 26.0% (± 2.5% SD; 9% CV); B17 = 25.3% (± 1.0% SD; 4% CV)). In contrast, the 'other N compounds' class had peak contributions at station B16 (33.1% (± 1.7% SD; 5% CV)), compared with lowest contributions at B13 and B14 (22.0% (± 1.0% SD; 5% CV) and 22.9% (± 0.3% SD; 1% CV) respectively). For polysaccharides the highest contributions were mid-way across the transect at B15 (23.5% (± 2.9% SD; 12% CV)), compared with mean values < 14.7% at the southernmost (B13 & B14) and northernmost stations (B16 & B17). Lowest alkylpyrrole contributions were at B15 (10.6% (± 0.8% SD; 8% CV)) with all other stations reporting values > 12.4%. The *n*-alkene/*n*-alkane doublets (C_{10} – C_{23}) had slightly higher contributions at station B16 (5.8% (± 0.6% SD; 11% CV) compared with lower contributions at the northernmost station (B17 = 4.7% (± 0.2% SD; 5% CV)) and stations to the south (B13 = 4.9% (± 0.2% SD; 4% CV); B14 = 5.2% (± 0.2% SD; 4% CV); B15 = 4.9% (± 0.5% SD; 9% CV)). All *n*-alkene/*n*-alkane doublet distributions showed a general declining trend across all stations from C_{10} to C_{22}, but there was greater variability in higher molecular weight even chain length *n*-alkanes in some replicates at stations B16 and B14 (Fig. 5). Consideration of replicate relative abundances for individual pyrolysis products (mean, SD, CV), supports the grouping approach of method A [12] for Barents Sea sediment samples (SI Table S1).

3.3.3. Method B

The lowest contribution of phenol quantified using a single abundant specific ion peak (Table 1) was at station B15 (11.8% (± 2.4% SD; 20% CV)) compared with highest contributions at B14 (20.6% (± 1.0% SD; 5% CV)) (Fig. 4b). For the 2 pyridines there was a gradual increasing trend north of B14, peaking at B16 (52.4% (± 3.5% SD; 7% CV)) but which again declined by B17 (45.6% (± 0.6% SD; 1% CV)). Dimethylbenzene was characterised by a gradual declining trend from the southernmost station (B13, 5.2% (± 0.4% SD; 7% CV)) to the northernmost station (B17, 3.1% (± 0.2% SD; 6% CV)). Similarly, methylcyclopentenone also featured a declining trend from B13 (4.2% (± 0.3% SD; 8% CV) northwards to B15 & B16 (1.6% (± 0.1% SD; 8% CV) and 1.6% (± 0.1% SD; 9% CV)), followed by an increase at the northernmost station, B17 (2.5% (± 0.2% SD; 7% CV)). The 2 furfurals had subtle variations with highest contributions at station B15 (35.4% (± 3.3% SD; 9% CV)) and the lowest contribution at B16 (21.1% (± 6.2% SD; 29% CV)). In contrast, the 2 aromatics had two minor increases in mean ratio at B13 (6.3% (± 0.5 SD; 8% CV)) and B16 (5.8% (± 0.8% SD; 14% CV), although these were within the error bars of all other samples (e.g. B14 = 4.6% (± 1.5% SD; 33% CV); B15 = 4.6% (± 1.07 SD; 37% CV). The grouping approach of method B [9] for Barents Sea sediment samples is supported by the replicate relative abundances for individual pyrolysis products (mean, SD, CV; SI Table S2).

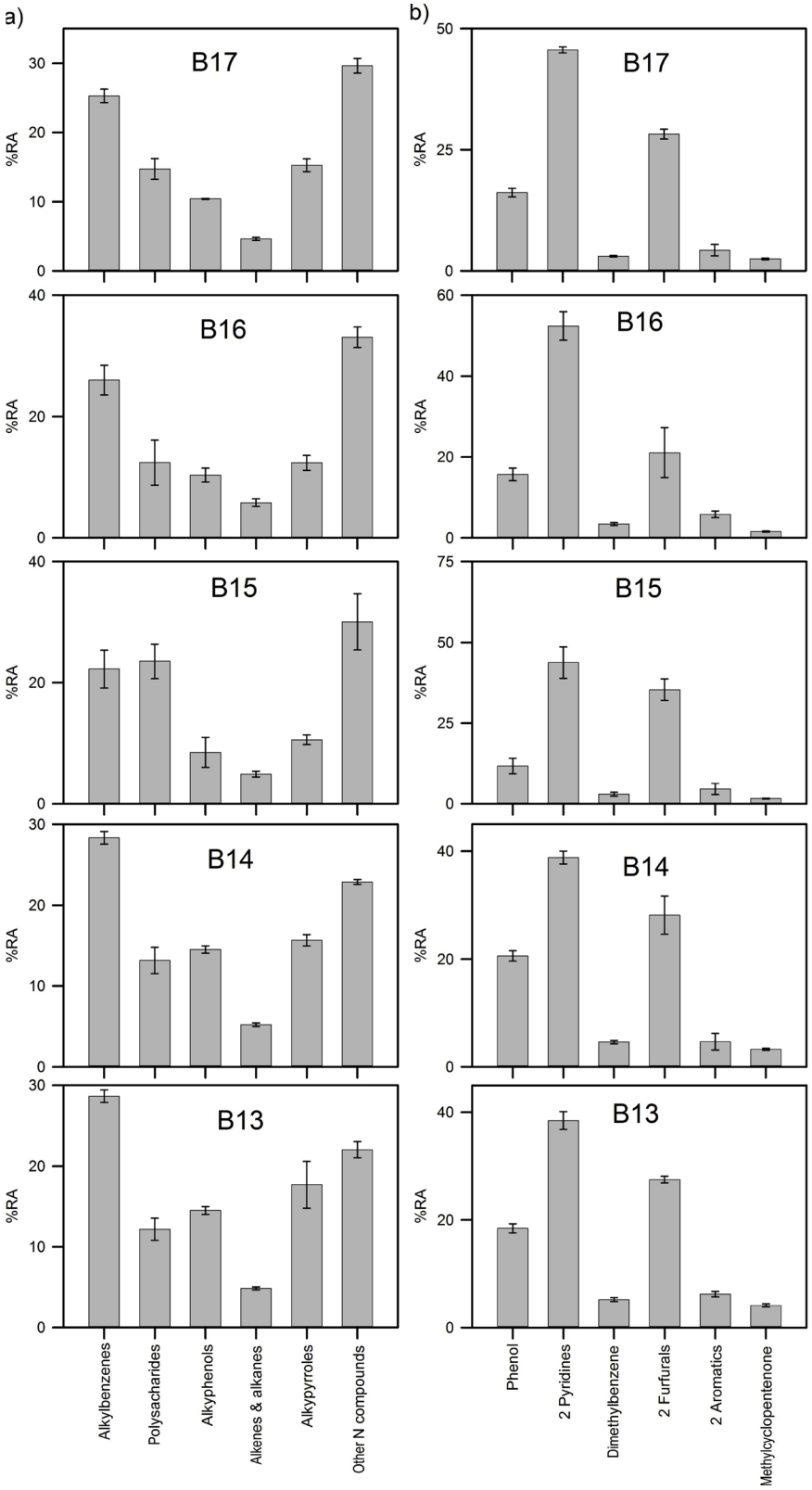

Fig. 3. a) Histograms showing groups of pyrolysis product compounds (alkylbenzenes, polysaccharides, alkylphenols, alkenes & alkanes, alkylpyrroles and other N containing compounds) in surface sediments analysed using Py-GC–MS compiled using method A. **b)** Histograms showing groups of compounds (phenol, 2 pyridines, dimethylbenzene, 2 furfurals, 2 aromatics and methylcyclopentenone) in surface sediments analysed using Py-GC–MS compiled using method B. Presented as relative abundances (RA) for stations B13 to B17. Error bars denote standard deviations for samples analysed in triplicate.

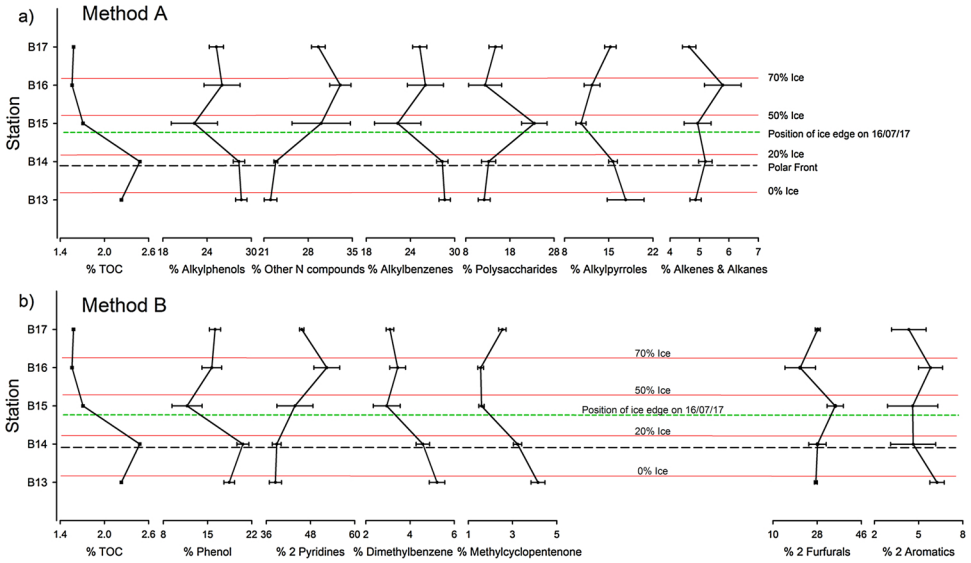

Fig. 4. %TOC and relative abundances of pyrolysis product compound class groups for methods A and B presented from north (B17) to south (B13) across the changing sea ice transect. Similar compound groups between methods A and B are aligned vertically (alkylphenols/phenol, other N compounds/2 pyridines, alkylbenzenes/dimethylbenzene and polysaccharides/methylcyclopentenone). Where compound groups differed between methods these are vertically separated (alkylpyrroles, alkenes & alkanes, 2 furfurals and 2 aromatics). Dashed line (black) indicates mean position of the Polar Front from Fossheim et al. [16]. Average percent ice cover (red lines) from Maiti et al. [17] and Keup-Thiel et al. [18]. Position of first ice margin (green dashed line) on 16/07/17 sourced from OSI SAF ice edge data (EUMETSAT). Error bars denote standard deviations for samples analysed in triplicate.

4. Discussion

There were fluctuations in the relative abundances of pyrolysis products across the N-S transect when using both methods (Fig. 4), but the differences between compound class (Fig. 3) were subtle when compared with studies which have focused on coastal to oceanic gradients [9]. The changes infer variations in macromolecular source inputs, predominantly from marine origins across the ice margin. Variability in pyrolysis product class composition across the N-S transect relates to both the seasonal ice edge, associated with phytoplankton blooms and nutrient release, together with the relative position of the Polar Front associated with Atlantic and Arctic water masses (Fig. 1). Spatial heterogeneity in primary production, water masses and the position of the ice edge cause complex and variable structural differences in zooplankton biomass [20,21], fish assemblages [16] and benthic communities [22] in the Barents Sea, affecting the macromolecular composition of the resulting sedimentary organic matter.

4.1. Spatial distribution of organisms in the Barents Sea

The copepod *Calanus finmarchicus* dominates the zooplankton biomass in the southern Barents Sea some of which is advected from the Norwegian Sea and grazed on by capelin [21]. Capelin predation on euphausiids is a key interrelationship, with the intensity of this varying between years [23]. At the ice-edge zooplankton feed on algal material released directly from ice melt and on the secondary phytoplankton bloom once melt has progressed [24]. This provides an excellent food source for copepods such *C. finmarchicus* which are present mainly at the Polar Front or further south in the Barents Sea [24]. This contrasts with amphipods which are abundant in the cooler Arctic water north of the Polar Front. Highest chlorophyll *a* phytoplankton bloom tends to be just south of the ice edge where Atlantic waters meet cooler Arctic waters, resulting in some water mass mixing and the availability of nutrients for primary production [20]. This contrasts with overall delivery of material from pelagic productivity in the southern sector of the Barents Sea which receives a relatively small proportion of material from pelagic productivity compared with central and northern sectors [17]. Zooplankton such as *C. finmarchicus* follow algal indicators closely, as evidenced by its abundance as far north as B14 in 2006 [20]. Fish species community also differs markedly south and north of the Polar Front [16]. Examples of fish found to be consistent with the Atlantic influenced southern Barents Sea include Haddock *(Melanogrammus aeglefinus)*, Norway pout *(Trisopterus esmarkii)* and Golden redfish *(Sebastes marinus)*. In contrast, examples of fish found to be consistent with the northern Barents Sea include Polar Cod (Boreogadus saida), Atlantic hookear sculpin *(Artediellus atlanticus)* and Eelpout (spp.) (*Lycodes* spp.) [16].

4.2. Changes in TOC content

TOC content was highest at station B14 which is close to the mean position of the Polar Front [16] and average ice cover of 20% [17]. Higher TOC at station B14 compared with further north can be explained by higher overall production, including production by mesozooplankton [20] and proximity to the position of the ice edge during sampling and average ice edge of 20% [17,18] (Fig. 4). Marginal ice zones are characterised by high production, where the seasonal retreat of the ice edge, although varied between years causes a highly productive and nutrient rich shallow mixed surface layer [22,25]. Additionally, proximity to the Polar Front can mean greater advection of mobile organisms to this area, including fish such as capelin and high levels of biomass from euphausiids [23], contributing to higher TOC in surface sediments.

4.3. Interpretation of changes from method A

The fluctuation in alkylphenol pyrolysis products around B15 could in principle have either terrestrial or algal origins (Fig. 4a). Where terrestrial inputs are considerable phenols have been suggested as representing lignin inputs [9,10] such as on the East Siberian Arctic shelf, where major river systems deliver allochthonous material. However, alkylphenols can also be of marine origin as they can be pyrolysis products of both proteins and polysaccharides, which are contained in broad classes of organisms, both within the water column and at the ocean floor [12,26]. Since there was an absence of catechol which would be expected if terrestrial tannins were a major input, the fluctuation in alkylphenols around B15 likely reflects lower input of recalcitrant material. B15 is proximal to both the position of the ice edge during sampling and close to the 50% mean ice cover marker (Figs. 1 & 4 a) and so the fluctuation is probably explained by a change in community structure around the ice edge. Diatoms dominate ice-edge phytoplankton blooms [27], helping to explain the slight proportional decrease in alkylphenols at B15. Phenolic compounds are particularly abundant in the cell walls of brown algae [28], which are probably transported by ocean currents less to B15 which is further from Atlantic currents from the south and Arctic currents from the north. Alkylbenzenes also were lower at station B15, with for example 1,2,3,4-tetramethylbenzene linked to carotenoids [12,29] and 1,2,3-

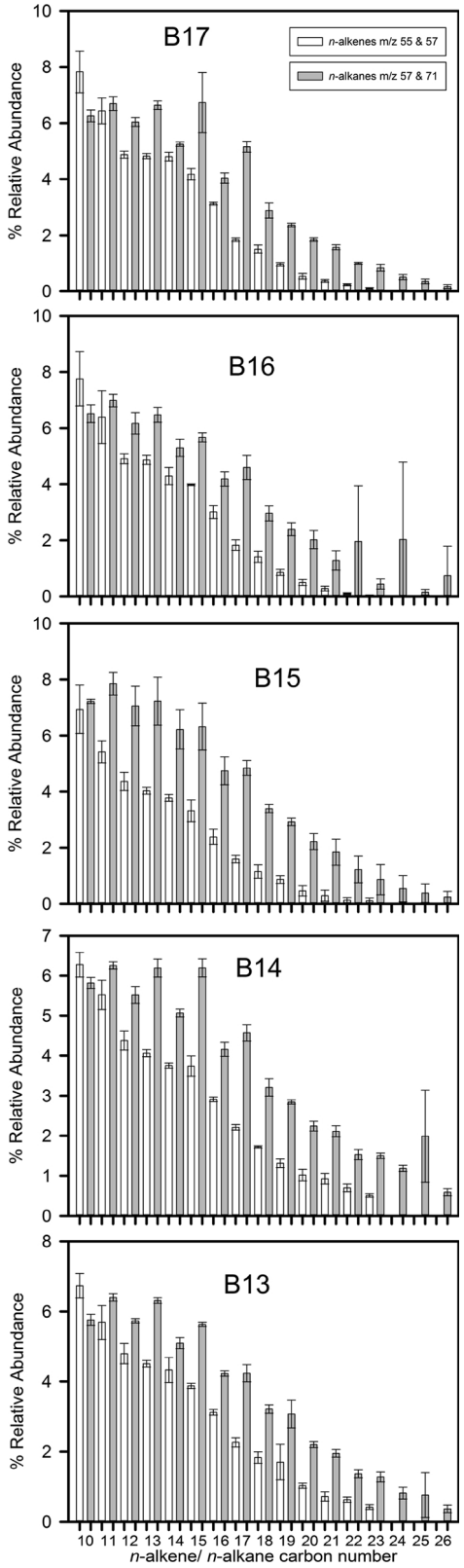

Fig. 5. Surface sediment sample *n*-alkene (*m/z* 55 & 57) and *n*-alkane (*m/z* 57& 71) distributions of pyrolysis products as relative abundances analysed using Py/GC–MS for stations B13 to B17. Chain lengths *n*-C_{10} to *n*-C_{23} are included in method A. Higher molecular weight *n*-C_{24} - *n*-C_{26} alkanes included in the chromatogram for completeness. Error bars denote standard deviations for samples analysed in triplicate.

trimethylbenzene to non-aromatic carotenoids which have lost methyl groups [12,30]. Similarly, alkylpyrroles were lower at B15 and include compounds such as pyrrole and 2-methylpyrrole which have broad source origins including chitin, algae and the organic linings of foraminifera [12]. Together these variations support the notion of a distinct ecosystem, at or close to the ice margin [24], north of the Polar Front.

Higher relative values of 'other N compounds' like indole and pyridine at stations B15 and B16 probably reflects a distinct compositional difference in marine inputs north of the ice edge margin and close to the 50–70% average ice cover markers (Figs. 1 & 4 a). For example, alkylpyridines have been detected in chitin from shrimp, zooplankton [12,31] but also to a lesser extent in ocean systems, in peptidoglycan which is abundant in bacteria [12,32]. Although observed zooplankton production annually is highest in the vicinity of the southernmost stations, this is highly varied between years [20,21] and the sampling strategy employed in these studies is unlikely to have fully captured activity at the ice edge. A likely explanation is the consumption of ice algae at the margin by zooplankton, a phenomenon that has been observed at sea ice margins in Hudson Bay, Canada [33] and the Canadian Resolute Passage [34]. Explaining high abundance of 'other N compounds' at B16 close to high average percent sea ice cover (Figs. 1 & 4 a), zooplankton such as copepods start feeding on ice algae when this remains attached to the ice bottom and are then supported during initial ice melt when most biomass is released and remains suspended in the upper water column [34]. Supporting this interpretation, the higher abundance of C_{10} to C_{23} *n*-alkene/*n*-alkane doublets at station B16 could be partly derived from algaenans which are resistant biopolymers in the cell walls of green algae, but also by geopolymerisation [12,35,36]. As this station was under broken sea ice during sampling in 2017 and is close to the 70% average ice cover marker (Figs. 1 & 4), it is possible that much of these contributions are linked to filamentous algae which bloom on and under sea ice when nutrient rich freshwater is released, stimulating diatoms such as *Melosira arctica* [37]. The presence of variable longer chain, even number C_{24}–C_{26} *n*-alkanes at station B16 and B14 (Fig. 5) together suggest an additional, distinct source at these stations, but an absence of odd over even predominance in these pyrolysates does not imply the source is unambiguously terrestrial.

The maxima in polysaccharides at station B15 (Fig. 4a) include increases in 2-furaldehyde and 5-methyl-2-furaldehyde [12,38] which are products of polysaccharides and are abundant in organisms in the upper ocean [39]. For polysaccharides differences in compositional distribution between stations probably mainly reflects differences in algal abundance and composition [40]. Increased polysaccharides close to the position of the open ice-edge is understandable as polysaccharides are high in the presence of semi-labile organic matter from phytoplankton blooms [41], which contribute to dominant DOM flux from decaying organic matter such as algae, often by heterotrophic processes [42].

4.4. Comparisons with method B

Similar to stations across the East Siberian Arctic shelf [9] all samples from the Barents Sea in this study were dominated by the 2 furfurals, 2 pyridines and phenol pyrolysis products which ranged from 84.4% (B13) to 90.9% (B15) (Fig. 3b). Despite reliance on just the compound phenol in method B (Fig. 4b) there was a similar shift around B15 to alkylphenols in method A (Fig. 4a). This shift occurs north of the Polar Front and close to the position of the ice edge observed during sampling (Fig. 1). Compared with locations on the East Siberian Arctic shelf where phenolic inputs may be elevated and a major source of phenols is riverine terrestrial plant material [9], the continental shelf east of Svalbard has fewer local potential inputs of less degraded material, helping to explain why these phenols are likely to be derived from marine protein and polysaccharides [12].

The increase in station B16 in pyridines (method B) broadly follows a similar shift to the 'other N compounds' class (method A) which also includes pyridine (Fig. 4). This likely reflects pyrolysis products of chitin from shrimp, zooplankton [12,31] and partly, but to a lesser extent peptidoglycan in bacteria [12,32]. As station B16 is between the 50–70% average ice cover markers (Figs. 1 & 4 b) the presence of seasonal melt, influences water mass structure increases nutrient availability, causing increased algal abundance at the ice margin. This has a resulting positive impact on zooplankton populations providing enhanced N-containing compounds and impacts on supported fish communities such as capelin [24]. The change in methylcyclopentenone (method B) which is lower at stations B15 and B16, follows a different trend compared with polysaccharides (method A). Some studies relate methylcyclopentenone to soil polysaccharides [9,10]. However, at these stations in the Barents Sea away from local terrestrial inputs, the source is likely to be mixed and predominantly marine.

4.5. Implications for ocean carbon cycling

The variations in macromolecular organic matter across the N-S transect primarily reflects the changing character of marine production across the observed ice edge (Figs. 1 & 4), north of the Polar Front which in particular become pronounced around stations B15 and B16. The ice-margin varies substantially in position seasonally and the uppermost surface layer of sediment (0.5 cm) is a time-integrated signal of multiple seasons. However, these stations are close to the ˜50% or greater average ice cover marker (Figs. 1 & 4) and so the ice edge can mediate community structure and the resulting macromolecular contributions. The Polar Front is also important along this N-S transect, marking the highest overall % TOC content close to B14. Here, warm and saline Atlantic waters meet cooler less saline Arctic water masses [43] facilitating marine production. The relative abundances of summed *n*-alkene/*n*-alkane doublets from the cell walls of living biomass, including algae, increases gradually from the southernmost station, significantly beyond the summer 2017 ice edge, but then sharply declines by the northernmost station (Fig. 4a). This suggests that the seasonal melt of summer sea ice shifts the composition of primary producers, altering the quality of carbon sequestered at the ocean floor. In turn, this carbon when transferred through the food web might stimulate secondary consumption by microbes and animals at the ocean floor [44], helping to explain these distinct transitions across the N-S transect. In future if the Polar Front moves northwards [5] and the extent of the ice edge does not reach as far south then deposition of more labile material (evidenced by deposition of N containing compounds) will move further north. Since the supply of labile organic material from the ice margin algal communities is associated with highly efficient carbon processing (evidenced by low %TOC at stations B15–B17), then initial carbon burial rates in the uppermost layers would be expected to increase overall, as areas of open ocean tend to have surface sediments with higher TOC (Fig. 4), and less efficient processing (stations B13 and B14). Regionally, this could lead to more burial of organic carbon in the surface sediments. Further research is required to quantify the stability of this labile organic carbon burial.

4.6. Comparison of techniques and future directions

Both approaches, used to investigate the macromolecular composition of organic matter across a S-N transect in the Barents Sea, yielded informative differences between stations. Including more compounds in the index (method A), where feasible, can help increase confidence in the compositional differences between stations. The selection of compound groupings need to be considered when interpreting trends as pyrolysis products (as often fragmented from larger molecules e.g. polysaccharides) are rarely unique to a specific organism. Despite this limitation, macromolecular analyses are more holistic and integrative of wider-scale changes in organic matter quality, when compared with changes in individual biomarkers (e.g. sterols [45]). Combining macromolecular analyses with pigment analyses would be useful to further refine which macromolecular compound classes are contributed to by specific algal groups, in a particular system. We did not find convincing changes in terrestrial inputs in our macromolecular analyses, notably because changes in alkylphenol relative values northwards in a marine setting can be derived from marine organisms (e.g. from proteins and polysaccharides). Searching for unambiguous *Sphagnum* and lignin terrestrial biomarkers either conventionally [46–48] or using thermally assisted hydrolysis and methylation (THM) in the presence of both unlabelled and ^{13}C-labelled tetramethylammonium hydroxide (TMAH) is one potential approach to quantify allochthonous inputs [15], however although oxic environments at the ocean floor during slow transport may degrade some of the more complex biomolecules, the C_{23} *n*-alkane, if dominant, potentially indicating OM contributions from *Sphagnum* and lignin should be more recalcitrant. Lignin phenols on sedimentary organic matter furthermore provide a useful tool to assess the level of degradation through the use of acid/aldehyde ratios [49,50]. An alternative approach would be to carry out macromolecular analyses on fraction separated organic matter (e.g. [8]), as it is possible different fractions may have differing terrestrial and marine sources and could enable quantification of potential long-distance transport. Despite these challenges, macromolecular compositions are likely to be useful in down-core models of organic matter reactivity and may help assess the potential for neo-geopolymerisation of macromolecular organic matter through organic matter diagenesis.

5. Conclusions

Changes in macromolecular composition of surface sediments across the S-N transect in the Arctic Barents Sea correspond to the varying marine benthic and pelagic communities (e.g. fish, plankton, ice algae & zooplankton) north of the Polar Front and across the variable sea ice margin. Macromolecular compositions from pyrolysis products are interpreted as primarily marine influenced given the transects location away from major terrigenous inputs, and the fact that changes were subtle when compared with macromolecular investigations on the East Siberian Arctic Shelf [9]. Changes in the relative amounts of labile N containing compounds (including pyridines) and high relative abundances of *n*-alkene/*n*-alkane doublets from the cell walls of living biomass, such as algae correspond to stations in the vicinity of greater average sea ice cover. With movement of the Polar Front and marginal ice further north, deposition of efficiently utilised labile material is likely to move northwards resulting in increased organic carbon in surface sediments under an open ocean. Both methods compared displayed insightful changes across the S-N transect, highlighting both that rapid screening is a useful approach, but that where possible adding additional compounds can help improve confidence. Future studies should identify if increased carbon deposited under an open ocean will be buried and if this is regionally significant, given the potential for weakening stratification associated with climate change, movement of the Polar Front northwards and a more Atlantic influenced northern Barents Sea.

Acknowledgements

This work resulted from the ChAOS project (NE/P00637X/1) part of the Changing Arctic Ocean programme, funded by UKRI Natural Environment Research Council (NERC). We would like to thank both the crew and science parties on board the RRS James Clark Ross cruise no. JR16006. We would also like to thank Bernard Bowler, Alex Charlton and Paul Donohoe for technical assistance at Newcastle University. We thank Christian März, Neil Gray, Robert Hilton, Sian Henley, Allyson Tessin, Johan Faust, Martin Solan, Steve Widdicombe and Laura Grange for insightful discussions which helped inspire interpretations of these results. We acknowledge the assistance of Jo

Hopkins who provided the base layer map and Phil Hwang who sourced sea ice position data (Fig. 1). We appreciate the input of three anonymous reviewers in improving earlier versions of this article.

Appendix A. Supplementary data

Supplementary material related to this article can be found, in the online version, at doi:https://doi.org/10.1016/j.jaap.2019.02.006.

References

[1] J.C. Stroeve, V. Kattsov, A. Barrett, M. Serreze, T. Pavlova, M. Holland, W.N. Meier, Trends in Arctic sea ice extent from CMIP5, CMIP3 and observations, Geophys. Res. Lett. 39 (2012) 1–7.

[2] D. Notz, J. Stroeve, Observed Arctic sea-ice loss directly follows anthropogenic CO_2 emission, Science 354 (2016) 747–750.

[3] M. Kędra, C. Moritz, E.S. Choy, C. David, R. Degen, S. Duerksen, I. Ellingsen, B. Górska, J.M. Grebmeier, D. Kirievskaya, D. van Oevelen, K. Piwosz, A. Samuelsen, J.M. Węsławski, Status and trends in the structure of Arctic benthic food webs, Polar Res. 34 (2015) 23775.

[4] E. Post, Implications of earlier sea ice melt for phenological cascades in arctic marine food webs, Food Webs 13 (2017) 60–66.

[5] S. Lind, R.B. Ingvaldsen, T. Furevik, Arctic warming hotspot in the northern Barents Sea linked to declining sea-ice import, Nat. Clim. Change 8 (2018) 634–639.

[6] B.I. Barton, Y.-D. Lenn, C. Lique, Observed atlantification of the Barents Sea causes the Polar Front to limit the expansion of winter sea ice, J. Phys. Oceanogr. 48 (2018) 1849–1866.

[7] S. Pabi, G.L. van Dijken, K.R. Arrigo, Primary production in the Arctic Ocean, 1998–2006, J. Geophys. Res. Oceans 113 (2008) 1–22.

[8] T. Tesi, I. Semiletov, O. Dudarev, A. Andersson, Ö. Gustafsson, Matrix association effects on hydrodynamic sorting and degradation of terrestrial organic matter during cross-shelf transport in the Laptev and East Siberian shelf seas, J. Geophys. Res. Biogeosci. 121 (2016) 731–752.

[9] R.B. Sparkes, A. Dogrul Selver, Ö. Gustafsson, I.P. Semiletov, N. Haghipour, L. Wacker, T.I. Eglinton, H.M. Talbot, B.E. Van Dongen, Macromolecular composition of terrestrial and marine organic matter in sediments across the East Siberian Arctic Shelf, Cryosphere 10 (2016) 2485–2500.

[10] L. Guo, I. Semiletov, Ö. Gustafsson, J. Ingri, P. Andersson, O. Dudarev, D. White, Characterization of Siberian Arctic coastal sediments: implications for terrestrial organic carbon export, Global Biogeochem. Cycl. 18 (2004).

[11] L. Guo, D.M. White, C. Xu, P.H. Santschi, Chemical and isotopic composition of high-molecular-weight dissolved organic matter from the Mississippi River plume, Mar. Chem. 114 (2009) 63–71.

[12] K.G.J. Nierop, G.-J. Reichart, H. Veld, J.S. Sinninghe Damsté, The influence of oxygen exposure time on the composition of macromolecular organic matter as revealed by surface sediments on the Murray Ridge (Arabian Sea), Geochim. Cosmochim. Acta 206 (2017) 40–56.

[13] K.A. Giles, S.W. Laxon, A.L. Ridout, Circumpolar thinning of Arctic sea ice following the 2007 record ice extent minimum, Geophys. Res. Lett. 35 (2008).

[14] J. Hopkins, The Changing Arctic Ocean Cruise JR16006, RRS James Clark Ross Cruise Report No. 51 30 June–8 August 2017, (2018) https://www.bodc.ac.uk/resources/inventories/cruise_inventory/reports/jr16006.pdf.

[15] M. Jakobsson, L. Mayer, B. Coakley, J.A. Dowdeswell, S. Forbes, B. Fridman, H. Hodnesdal, R. Noormets, R. Pedersen, M. Rebesco, H.W. Schenke, Y. Zarayskaya, D. Accettella, A. Armstrong, R.M. Anderson, P. Bienhoff, A. Camerlenghi, I. Church, M. Edwards, J.V. Gardner, J.K. Hall, B. Hell, O. Hestvik, Y. Kristoffersen, C. Marcussen, R. Mohammad, D. Mosher, S.V. Nghiem, M.T. Pedrosa, P.G. Travaglini, P. Weatherall, The International Bathymetric Chart of the Arctic Ocean (IBCAO) Version 3.0, Geophys. Res. Lett. 39 (2012).

[16] M. Fossheim, E.M. Nilssen, M. Aschan, Fish assemblages in the Barents Sea, Mar. Biol. Res. 2 (2006) 260–269.

[17] K. Maiti, J. Carroll, C.R. Benitez-Nelson, Sedimentation and particle dynamics in the seasonal ice zone of the Barents Sea, J. Mar. Syst. 79 (2010) 185–198.

[18] E. Keup-Thiel, H. Göttel, D. Jacob, Regional climate simulations for the Barents Sea region, Boreal Environ. Res. 11 (2006) 329–339.

[19] G.D. Abbott, E.Y. Swain, A.B. Muhammad, K. Allton, L.R. Belyea, C.G. Laing, G.L. Cowie, Effect of water-table fluctuations on the degradation of *Sphagnum* phenols in surficial peats, Geochim. Cosmochim. Acta 106 (2013) 177–191.

[20] P. Dalpadado, K.R. Arrigo, S.S. Hjøllo, F. Rey, R.B. Ingvaldsen, E. Sperfeld, G.L. van Dijken, L.C. Stige, A. Olsen, G. Ottersen, Productivity in the Barents Sea-response to recent climate variability, PLoS One 9 (2014) e95273.

[21] P. Dalpadado, R. Ingvaldsen, A. Hassel, Zooplankton biomass variation in relation to climatic conditions in the Barents Sea, Polar Biol. 26 (2003) 233–241.

[22] T. Tamelander, P.E. Renaud, H. Hop, M.L. Carroll, W.G. Ambrose Jr., K.A. Hobson, Trophic relationships and pelagic–benthic coupling during summer in the Barents Sea Marginal Ice Zone, revealed by stable carbon and nitrogen isotope measurements, Mar. Ecol. Prog. Ser. 310 (2006) 33–46.

[23] E.L. Orlova, A.V. Dolgov, P.E. Renaud, M. Greenacre, C. Halsband, V.A. Ivshin, Climatic and ecological drivers of euphausiid community structure vary spatially in the Barents Sea: relationships from a long time series (1952–2009), Front. Mar. Sci. 1 (2015).

[24] F. Rey, H.R. Skjoldal, A. Hassel, Seasonal Development of Plankton in the Barents Sea: A Conceptual Model, ICES, 1987.

[25] H.J. Niebauer, V. Alexander, S. Henrichs, Physical and biological oceanographic interaction in the spring bloom at the Bering Sea marginal ice edge zone, J. Geophys. Res: Ocean 95 (1990) 22229–22241.

[26] J.D.H. Van Heemst, S. Peulve, J.W. De Leeuw, Novel algal polyphenolic biomacromolecules as significant contributors to resistant fractions of marine dissolved and particulate organic matter, Org. Geochem. 24 (1996) 629–640.

[27] E.E. Syvertsen, Ice algae in the Barents Sea: types of assemblages, origin, fate and role in the ice-edge phytoplankton bloom, Polar Res. 10 (1991) 277–288.

[28] M.E. Schoenwaelder, M.N. Clayton, The presence of phenolic compounds in isolated cell walls of brown algae, Phycologia 38 (1999) 161–166.

[29] M.J.L. Hoefs, J.S. Sinninghe Damste, G.J. De Lange, J.W. de Leeuw, Changes in kerogen composition across an oxidation front in Madeira Abyssal Plain turbidites as revealed by pyrolysis GC-MS, Proc. Ocean Drill. Prog. Sci. Results 157 (1998) 591–607.

[30] W.A. Hartgers, J.S.S. Damsté, J.W. de Leeuw, Geochemical significance of alkylbenzene distributions in flash pyrolysates of kerogens, coals, and asphaltenes, Geochim. Cosmochim. Acta 58 (1994) 1759–1775.

[31] B. Arthur Stankiewicz, P.F. van Bergen, I.J. Duncan, J.F. Carter, D.E.G. Briggs, R.P. Evershed, Recognition of chitin and proteins in invertebrate cuticles using analytical pyrolysis/gas chromatography and pyrolysis/gas chromatography/mass spectrometry, Rapid Commun. Mass Spectrom. 10 (1996) 1747–1757.

[32] A.P. Snyder, J.P. Dworzanski, A. Tripathi, W.M. Maswadeh, C.H. Wick, Correlation of mass spectrometry identified bacterial biomarkers from a fielded pyrolysis-gas chromatography-ion mobility spectrometry biodetector with the microbiological gram stain classification scheme, Anal. Chem. 76 (2004) 6492–6499.

[33] J. Runge, R.G. Ingram, Under-ice feeding and diel migration by the planktonic copepods Calanus glacialis and Pseudocalanus minutus in relation to the ice algal production cycle in southeastern Hudson Bay, Canada, Mar. Biol. 108 (1991) 217–225.

[34] C. Michel, L. Legendre, R. Ingram, M. Gosselin, M. Levasseur, Carbon budget of sea-ice algae in spring: Evidence of a significant transfer to zooplankton grazers, J. Geophys. Res. Oceans 101 (1996) 18345–18360.

[35] J.W. De Leeuw, C. Largeau, A review of macromolecular organic compounds that comprise living organisms and their role in kerogen, coal, and petroleum formation, in: M.H. Engel, S.A. Macko (Eds.), Organic Geochemistry, Springer, 1993, pp. 23–72.

[36] S. Derenne, F. Le Berre, C. Largeau, P. Hatcher, J. Connan, J.F. Raynaud, Formation of ultralaminae in marine kerogens via selective preservation of thin resistant outer walls of microalgae, Org. Geochem. 19 (1992) 345–350.

[37] A. Boetius, S. Albrecht, K. Bakker, C. Bienhold, J. Felden, M. Fernández-Méndez, S. Hendricks, C. Katlein, C. Lalande, T. Krumpen, M. Nicolaus, I. Peeken, B. Rabe, A. Rogacheva, E. Rybakova, R. Somavilla, F. Wenzhöfer, Export of algal biomass from the melting Arctic sea ice, Science 339 (2013) 1430–1432.

[38] A. van Der Kaaden, J. Haverkamp, J.J. Boon, J.W. De Leeuw, Analytical pyrolysis of carbohydrates: I. Chemical interpretation of matrix influences on pyrolysis-mass spectra of amylose using pyrolysis-gas chromatography-mass spectrometry, J. Anal. Appl. Pyrol. 5 (1983) 199–220.

[39] J.D. Pakulski, R. Benner, Abundance and distribution of carbohydrates in the ocean, Limnol. Oceanogr. 39 (1994) 930–940.

[40] H. Sakugawa, N. Handa, Chemical studies on dissolved carbohydrates in the water samples collected from the North Pacific and Bering Sea, Oceanol. Acta 8 (1985) 185–196.

[41] J. Piontek, N. Händel, C. De Bodt, J. Harlay, L. Chou, A. Engel, The utilization of polysaccharides by heterotrophic bacterioplankton in the Bay of Biscay (North Atlantic Ocean), J. Plankton Res. 33 (2011) 1719–1735.

[42] J. Rich, M. Gosselin, E. Sherr, B. Sherr, D.L. Kirchman, High bacterial production, uptake and concentrations of dissolved organic matter in the Central Arctic Ocean, Deep. Sea Res. Part II Top. Stud. Oceanogr. 44 (1997) 1645–1663.

[43] L. Oziel, J. Sirven, J.C. Gascard, The Barents Sea frontal zones and water masses variability (1980–2011), Ocean Sci. 12 (2016) 169–184.

[44] J.J. Middelburg, Review and syntheses: to the bottom of carbon processing at the seafloor, Biogeosciences 15 (2018) 413–427.

[45] J.K. Volkman, A review of sterol markers for marine and terrigenous organic matter, Org. Geochem. 9 (1986) 83–99.

[46] J. Schellekens, R. Bindler, A. Martínez-Cortizas, E.L. McClymont, G.D. Abbott, H. Biester, X. Pontevedra-Pombal, P. Buurman, Preferential degradation of polyphenols from *Sphagnum* – 4-Isopropenylphenol as a proxy for past hydrological conditions in *Sphagnum*-dominated peat, Geochim. Cosmochim. Acta 150 (2015) 74–89.

[47] J. Schellekens, J.A. Bradley, T.W. Kuyper, I. Fraga, X. Pontevedra-Pombal, P. Vidal-Torrado, G.D. Abbott, P. Buurman, The use of plant-specific pyrolysis products as biomarkers in peat deposits, Quat. Sci. Rev. 123 (2015) 254–264.

[48] D. Edwards, G. Ewbank, G.D. Abbott, Flash pyrolysis of the outer cortical tissues in Lower Devonian Psilophyton dawsonii, Bot. J. Linn. Soc. 124 (1997) 345–360.

[49] J. Holtvoeth, T. Wagner, C.J. Schubert, Organic matter in river-influenced continental margin sediments: the land-ocean and climate linkage at the Late Quaternary Congo fan (ODP Site 1075), Geochem. Geophys. Geosyst. 4 (2003).

[50] S.L. Mason, T.R. Filley, G.D. Abbott, The effect of afforestation on the soil organic carbon (SOC) of a peaty gley soil using on-line thermally assisted hydrolysis and methylation (THM) in the presence of 13C-labelled tetramethylammonium hydroxide (TMAH), J. Anal. Appl. Pyrolysis 85 (2009) 417–425.